A dual anchoring strategy for the localization and activation of artificial metalloenzymes based on the biotin-streptavidin technology.

Jeremy M. Zimbron, Tillmann Heinisch, Maurus Schmid, Didier Hamels, Elisa S. Nogueira, Tilman Schirmer and Thomas R. Ward*

Biozentrum and Department of Chemistry, University of Basel, CH-4056 Basel, Switzerland

e-mail: thomas.ward@unibas.ch

ABSTRACT: Artificial metalloenzymes result from anchoring an active catalyst within a protein environment. Towards this goal, various localization strategies have been pursued: covalent-, supramolecular- or dative anchoring. Herein we show that introduction of a suitably positioned histidine residue contributes to firmly anchor via a dative bond a biotinylated rhodium pianostool complex within streptavidin. The in-silico design of the artificial metalloenzyme was confirmed by X-ray crystallography. The resulting artificial metalloenzyme displays significantly improved catalytic performance, both in terms of activity and selectivity in the transfer hydrogenation of imines. Depending on the position of the histidine residue, both enantiomers of the salsolidine product can be obtained.

INTRODUCTION

In recent years, the field of artificial metalloenzymes has attracted increasing attention as alternative to the more traditional heterogeneous-, homogeneous- and enzymatic catalysts.[1-6] Artificial metalloenzymes result from incorporation of a catalytically competent organometallic moiety within a protein scaffold. Towards this goal, covalent-, dative- and supramolecular anchoring strategies have been pursued.

We and others have been relying on the biotin-(strept)avidin technology to create artificial metalloenzymes.[7-11] The catalytic performance of these can be optimized relying on either chemical or genetic means.[12] Recent structural and kinetic data of artificial metalloenzymes based on the biotin-streptavidin technology highlighted that: i) the metal is located in a shallow energy minimum resulting in poorly localized metal moieties (as reflected by low occupancy in the X-ray structure); ii) the presence of second coordination sphere provided by streptavidin significantly influences the selectivity of the resulting artificial metalloenzymes.[13] In contrast, the activity (TOF, TON) is only moderately affected upon incorporation in streptavidin. This presents a serious limitation towards the implementation of directed evolution protocols of artificial metalloenzymes. Indeed, it requires the precise quantification of the protein as any non-protein bound metal would lead to an erosion of enantioselectivity.[10] We speculated that, in addition to the biotin anchor, a properly positioned histidine residue provided by streptavidin may contribute to firmly localize the metal-containing biotinylated cofactor and to activate the precatalyst (Scheme 1). The groups of Lu and Watanabe independently pioneered an anchoring strategy to introduce Schiff-base complexes within apo-myoglobin. In both strategies, the Schiff-base complex was anchored thanks to a dative bond with the proximal histidine 93.[14,15] In addition, Lu and coworkers introduced two cysteine residues that further contributed to firmly localize the artificial cofactor thanks to the formation of two disulfide bonds with the Schiff-base.[14] Compared to the artificial metalloenzyme lacking the disulfide bridges, the dually anchored artificial metalloenzymes displayed improved sulfoxidase activity.[14] Inspired by this elegant study, we present our efforts towards the design and application of a dually anchored (i.e. dative and supramolecular) artificial metalloenzyme for the reduction of prochiral imines.

RESULTS AND DISCUSSION

Design considerations. With the aim of generating a widely applicable d^6-pianostool complex for a variety of catalytic applications upon introduction in streptavidin (Sav hereafter), we set out to link the biotin anchor to the cyclopentadienyl moiety. This strategy leaves three coordination sites available for catalysis and/or activation via additional ligands (Scheme 1). In order to gain a semi-quantitative insight on the position of the biotinylated pianostool complex **5** upon incorporation within Sav and which amino acid position may be amenable to bind to the metal upon mutation to a histidine, docking simulations were performed. All X-ray crystal structures containing a biotinylated metal complex obtained within the Ward group indicate that the position of the biotin moiety and the C_αs of the protein are essentially invariant, irrespective of the nature of the metal complex bound to biotin.[13,16-18] Therefore, the DFT-optimized structure of the monomeric biotinylated complex [η^5-(Biot-**2**)$RhCl_2(H_2O)$] was manually positioned into WT Sav (PDB code 1MK5) by superimposing the biotin anchor of the complex to the native biotin present in the crystal structure. Simulations were performed in NAMD[19] using the CHARMM27 force-field[20] with parameters developed in our group[21] or elsewhere[22] (See SI for details).

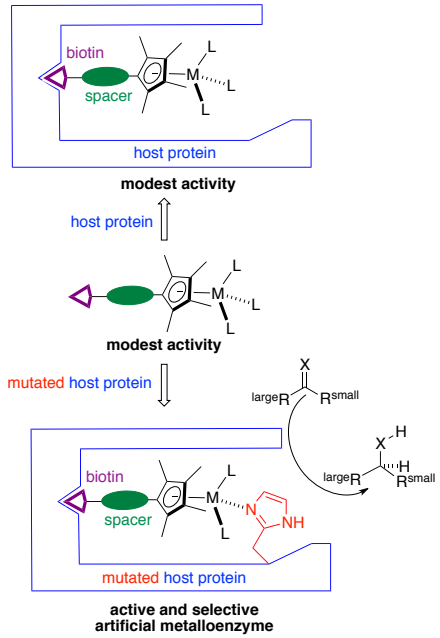

Scheme 1 Dual anchoring strategy to localize and activate a biotinylated pianostool catalyst precursor upon incorporation into streptavidin.

The system was subsequently minimized for 1000 Conjugate Gradient steps, followed by a short molecular dynamics simulation (Langevin NVT ensemble) of 500 ps. The structure in the final snapshot was minimized again for 1000 steps to yield the docked structure. Only the aquo complex [η^5-(Biot-**2**)$RhCl_2(H_2O)$] and atoms within 5 Å of the complex were allowed to relax during the simulation, the rest of the protein was kept frozen. The resulting structure is depicted in Figure 1 a. With respect to the rhodium-center, the two closest lying $C_ß$ atoms are provided by S112 (5.62 Å) and K121 (6.09 Å of the adjacent monomer). Next, a histidine residue was introduced at either position S112 or K121. The rhodium-bound water was replaced by a bond to the $N_ε$ histidine and the procedure described above was applied yielding [(η^5-Biot-**2**)$RhCl_2$] **5** ⊂ S112H Sav and [(η^5-Biot-**2**)$RhCl_2$] **5** ⊂ K121H Sav (Figure 1 b and 1 c respectively).

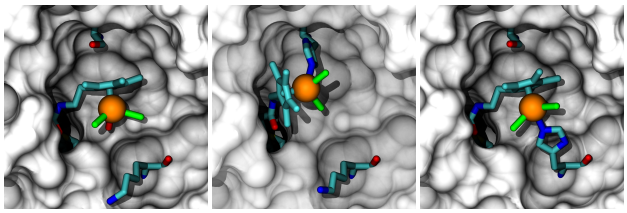

(a) **(b)** **(c)**

Figure 1 Docked structure of [η^5-(Biot-**2**)$RhCl_2(H_2O)$] ⊂ WT Sav (a); [(η^5-Biot-**2**)$RhCl_2$] **5** ⊂ S112H Sav (b) and [(η^5-Biot-**2**)$RhCl_2$] **5** ⊂ K121H Sav (the His is provided by the adjacent Sav monomer of the homotetrameric structure)(c). The pianostool complex and streptavidin's side-chains at positions 112 and 121 are displayed as stick representation, Sav as solvent accessible surface.

These simulations thus suggest that an ethylene spacer between the Cp*- and the biotin moieties positions the metal center in an environment, suitable for additional dative anchoring to a histidine side chain upon mutation of either S112H or K121H. Similar docking simulations were performed for complexes bearing either a methylene- or a propylene spacer in the presence of WT Sav. In both cases however, inspection of the docked structure revealed a less propitious environment for dative anchoring to an amino acid side chain of streptavidin: For the methylene spacer, steric hindrance between the docked ligand and the protein are observed whereas the propylene spacer projects the metal out of the biotin-binding vestibule (See SI).

Synthesis. Having identified a suitable spacer between the biotin anchor and the Cp* moiety, the corresponding d^6-piano stool complexes were synthesized. For this purpose, tetramethylcyclopentenone **1** was used as starting material for the synthesis of the cyclopentadienyl precursor H-**2** according to a slightly modified protocol of Teuben and coworkers.[23] Reaction with $RhCl_3·(H_2O)_n$ or with $[Ir(COD)Cl]_2$, followed by an *in-situ* oxidation with HCl, yielded the dinuclear pianostool complexes [η^5-(**2**)$RhCl_2]_2^{2+}$ **3** and [η^5-(**2**)$IrCl_2]_2^{2+}$ **4**, respectively.[24,25] Subsequent biotinylation using the pentafluorophenylester of biotin, allowed the isolation of the analytically pure, dimeric, [η^5-(Biot-**2**)$RhCl_2]_2$ $\mathbf{5_2}$ and [η^5-(Biot-**2**)$IrCl_2]_2$ $\mathbf{6_2}$ respectively (See SI for details).

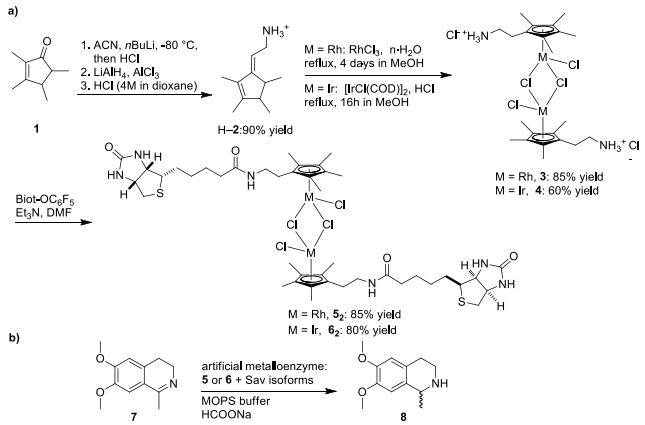

Scheme 2 Synthesis of biotinylated pianostool complexes (a) and asymmetric transfer hydrogenation conditions used towards the production of salsolidine **8** (b).

Catalysis. As model reaction, we selected the asymmetric transfer hydrogenation (ATH) of the prochiral imine **7** using biotinylated dimeric catalyst precursors $\mathbf{5_2}$ and $\mathbf{6_2}$. This reaction is frequently used as a benchmark as it offers a straightforward access to the alkaloid salsolidine **8** (Scheme 2b).[26] Selected results are collected in Table 1 and can be summarized as follows:

1) The iridium catalyst precursor [η^5-(Biot-**2**)$IrCl_2]_2$ $\mathbf{6_2}$ leads to higher conversions than the rhodium congener [η^5-(Biot-**2**)$RhCl_2]_2$ $\mathbf{5_2}$. The same trend applies upon incorporation in WT Sav albeit with reduced conversions (Entries 1-4). These results are in agreement with the findings of Ogo and coworkers by which $[Cp^*Ir(H_2O)_3]^{2+}$ is a significantly more active transfer hydrogenation catalyst than $[Cp^*Rh(H_2O)_3]^{2+}$.[27]

2) The presence of a histidine residue at position S112 Sav has a dramatic effect on the activity and the selectivity of the ATH. Salsolidine **8** is produced in 95% conversion and 41% ee (*S*) using [η^5-(Biot-**2**)$RhCl_2$] **5** ⊂ S112H at 55 °C and pH 6.5. The activity and the selectivity can be further improved upon lowering the pH to 5.0 (quantitative conversion with 1 mol % catalyst **5** and 55% ee (*S*)) (Table 1, entries 5 and 6). In

stark contrast, the presence of a histidine residue at position S112H has a detrimental effect on ATH with iridium (Table 1, entry 9). These results corroborate those of both Süss-Fink and Himeda whereby the transfer hydrogenase activity of $[Cp^*Rh(diimine)Cl]^+$ is reportedly higher than that of $[Cp^*Ir(diimine)Cl]^+$ (diimine = phenanthroline or 2,2'-bipyridine respectively).[28-29]

3) Introduction of other coordinating amino acids bearing soft donors (eg. cysteine or methionine, Table 1, entries 15 and 18) at position S112 affords salsolidine in high yield albeit low enantioselectivity. Again here, we speculate that the metal is activated by coordination to a suitably positioned soft amino acid residue. Docking of $[\eta^5$-(Biot-**2**)$RhCl_2]$ **5** ⊂ S112M indeed suggests that dative anchoring is likely (See SI).

4) Introduction of a histidine residue at position K121H Sav affords (*R*)-salsolidine **8** in up to 79% ee using the rhodium catalyst at 55 °C (Table 1, entries 10 and 11). Again here, *rac*-**8** is produced with the iridium catalyst in the presence of K121H. Lowering the temperature leads, for both S112H and K121H mutants and in the presence of the rhodium catalyst, to a decrease in enantioselectivity (Table 1, entries 7-8 and 12-13). This suggests that the $\Delta G^{\ddagger}$ term is dominated by the entropy contribution $\Delta S^{\ddagger}$.

5) All point mutants tested devoid of a histidine at either position S112 or K121 afforded nearly racemic salsolidine **8** (ee < 20%) (Table 1, entries 15-19). Interestingly, the double mutant S112H-K121H Sav gave very low levels of enantioselectivity (Table 1 entry 20). We speculate that, in the presence of the double mutant, the biotinylated cofactor binds indiscriminately, and thus in equimolar amounts, to either of S112H- and K121H-histidines, thus resulting in the production of (*rac*)-**8**.

6) Compared to $[\eta^5$-(Biot-**2**)$RhCl_2]$ **5** ⊂ WT Sav, both histidine bearing artificial metalloenzymes $[\eta^5$-(Biot-**2**)$RhCl_2]$ **5** ⊂ S112H Sav and $[\eta^5$-(Biot-**2**)$RhCl_2]$ **5** ⊂ K121H display increased turnover frequencies: 1 $hour^{-1}$ for the WT Sav compared to 6 $hour^{-1}$ for both S112H and K121H mutants.

Table 1 Selected results for the asymmetric transfer hydrogenation of prochiral imine **7** catalyzed by artificial metalloenzymes.

entry	$[(\eta^5$-Biot-L)$MCl_2]_2$	Sav isoform	Temp (°C)	pH	M loading	conv. (%)	ee (%)
1	Rh	–	55	6.5[a]	2%	26	rac.
2	Ir	–	55	6.5[a]	2%	87	rac.
3	Rh	WT	55	6.5[a]	2%	18	rac.
4	Ir	WT	55	6.5[a]	2%	60	6 (*S*)
5	Rh	S112H	55	6.5[a]	2%	95	41 (*S*)
6	Rh	S112H	55	5.0[b]	1%	quant.	55 (*S*)
7	Rh	S112H	25	5.0[c]	2%	85	52 (*S*)
8	Rh	S112H	5	5.0[b]	1%	5	45 (*S*)
9	Ir	S112H	55	6.5[a]	2%	27	11 (*S*)
10	Rh	K121H	55	6.5[a]	2%	95	50 (*R*)
11	Rh	K121H	55	5.0[b]	1%	quant.	79 (*R*)
12	Rh	K121H	25	5.0[c]	2%	25	50 (*R*)
13	Rh	K121H	5	5.0[b]	1%	5	50 (*R*)
14	Ir	K121H	55	6.5[a]	2%	37	rac.
15	Rh	S112C	55	6.5[a]	2%	93	14 (*S*)
16	Rh	S112E	55	6.5[a]	2%	26	rac.
17	Rh	S112K	55	6.5[a]	2%	40	13 (*S*)
18	Rh	S112M	55	6.5[a]	2%	98	19 (*R*)
19	Rh	K121N	55	6.5[a]	2%	44	rac.
20	Rh	S112H-121H	55	6.5[a]	2%	40	9 (*R*)

[a]The reaction was carried out in a MOPS buffer at pH 6.5 using HCOONa as hydride source: 2 mol % monomeric biotinylated catalyst **5** or **6** (458 μM final metal concentration), 4 mol % biotin binding sites (916 μM final concentration) and substrate **7** (22.9 mM final concentration, total reaction volume 200 μL) (See SI).

[b]The reaction was carried out in a MOPS buffer at pH 5.0 using HCOONa as hydride source: 1 mol % monomeric biotinylated catalyst **5** or **6** (458 μM final metal concentration), 2 mol % biotin binding sites (916 μM final concentration) and substrate **7** (45.8 mM final concentration, total reaction volume 200 μL) (See SI).

[c]The reactions were carried out in a MOPS buffer at pH 5.0 using HCOONa as hydride source: 2 mol% monomeric biotinylated complex **5** (680 μM final metal concentration and 2.64 mol % biotin binding sites (corresponding to 916 μM biotin binding sites) and substrate **7** (34 mM final concentration, total reaction volume of 200 μL).

Structural Characterization. Next, X-ray crystal structure analyses were carried out with the most selective artificial metalloenzymes: [(η^5-Biot-**2**)$RhCl_2$] ⊂ S112H and [η^5-(Biot-**2**)$RhCl_2$] ⊂ K121H. Crystals of apo-streptavidin mutants S112H and K112H were soaked at pH 6 with an excess of complex [η^5-(Biot-**2**)$RhCl_2$]$_2$ **5$_2$**. The crystal structures of **5** ⊂ S112H and **5** ⊂ K121H could be solved to 2.4 Å and 1.8 Å resolution, respectively. Both structures contained strong electron density in the Fo-Fc map in the biotin-binding pocket and in the proximity of the histidine residue either at position H112 or H121. The monomeric complexes [η^5-(Biot-**2**)Rh]$^{2+}$ and [η^5-(Biot-**2**)RhCl]$^+$ were fitted into the electron densities localized around H112 and H121' respectively (Figure 2 and SI Figure 3). As highlighted by the docking simulations, the H121' of an adjacent monomer in homotetrameric streptavidin lies closest to the Rh in the **5** ⊂ K121H structure, Figure 1 c and 2b. Dative bonds were modeled between rhodium and the corresponding histidine: Rh–Nδ^{His112} 2.3 Å for **5** ⊂ S112H and Rh–N$\varepsilon^{His121'}$ 2.3 Å for **5** ⊂ K121H. The Rh····Rh distances between two biotinylated molecules bound to neighboring symmetry-related Sav monomers are 9.5 Å and 9.2 Å for **5** ⊂ S112H and **5** ⊂ K121H, respectively. The position of the complexes in the S112H and K121H isoforms differs by an approximate 180° rotation of the Cp*Rh(Cl) group along an axis pointing towards the biotin binding pocket. Compared to the X-ray structure of biotin-loaded Sav (pdb code 1stp), the rmsd of the C_α for **5** ⊂ S112H and **5** ⊂ K121H are 0.247 Å and 0.214 Å respectively, highlighting the minimal structural reorganization of the host protein upon introduction of he biotinylated cofactor.

For the complex bound to S112H, no additional electron density to complete the three-legged pianostool geometry could be detected whereas the presence of a chloride ligand was apparent for the K121H structure.

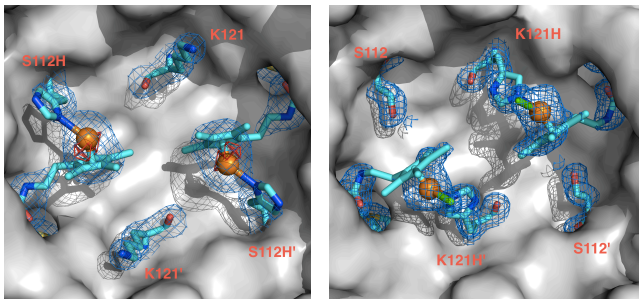

a) **b)**

Figure 2 Close-up view of the X-ray crystal structure of [(η^5-Biot-**2**)Rh]$^{2+}$ ⊂ S112H Sav (a); and [(η^5-Biot-**2**)RhCl]$^+$ ⊂ K121H Sav (b). The protein is displayed as surface representation and the ligand molecules as well as residues 112 and 121 in stick representation. The positions of ligand molecules are indicated by the 2Fo-Fc electron density (blue, contoured at 1.0 σ) and anomalous difference density (red, contoured at 4 σ, due to weak absorption at a wavelength of 1.00 Å no anomalous density was observed in structure [(η^5-Biot-**2**)RhCl]$^+$ ⊂ K121H Sav). Rhodium is colored in orange and chlorine in green. Residues H121' and K121' are provided by the adjacent Sav monomer.

Comparison of the docked vs. X-ray structures of both mutant metalloenzymes reveals a semi-quantitative agreement: the computed rmsd = 3.4 Å for the pianostool atoms in **5** ⊂ S112H and 2.1 Å for the pianostool atoms in **5** ⊂ K121H. Upon anchoring the catalyst via Rh–Nδ^{His112}, as found in the X-ray structure (Figure 2a), the rmsd decreases to 1.23 Å (See SI). These deviations can by-and-large be traced back to the differing conformation adopted by the ethylene spacer (docked vs. X-ray, See SI). Despite this, the docking proved predictive enough to successfully engineer dative anchoring sites for the biotinylated cofactor. A full parametrization of the biotinylated Rh-pianostool moiety will be required to yield more reliable docking results.

Inspection of the steric environment enforced by the host protein around the [(η^5-Biot-**2**)$RhCl_2$] ⊂ S112H and [η^5-(Biot-**2**)$RhCl_2$] ⊂ K121H reveals a "pseudo-mirror image relationship" between the two mutant artificial metalloenzymes, thus accounting for the production of (*S*)-**8** and (*R*)-**8** respectively (Figure 3 a and b).

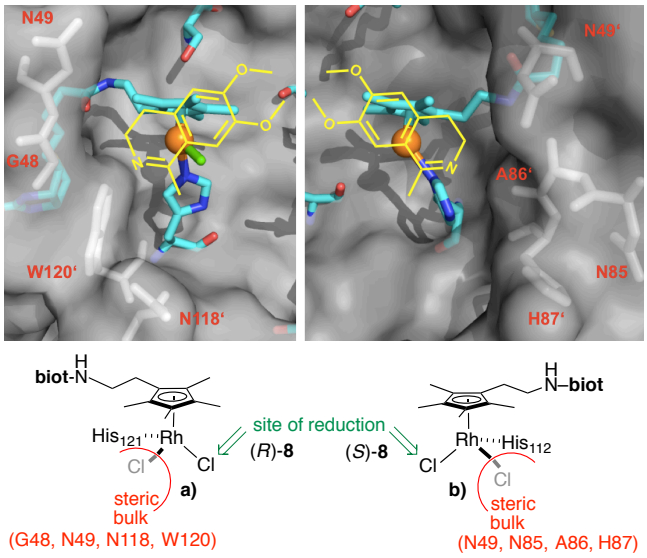

Figure 3 Schematic representation of [(η^5-Biot-**2**)$RhCl_2$] ⊂ K121H Sav (a); and [(η^5-Biot-**2**)$RhCl_2$] ⊂ S112H Sav (b). The steric bulk provided by Sav creates "pseudo mirror-image environments" around the two transfer hydrogenases, thus favouring the approach of opposite prochiral faces of the imine substrate (in yellow).

OUTLOOK

Dual anchoring of a biotinylated three-legged rhodium pianostool complex affords an artificial transfer hydrogenase. It was shown that coordination of the catalyst precursor to a suitably positioned histidine residue has a significant impact on the catalyst's performance, both in terms of activity and of selectivity. The computational design towards the identification of the spacer-length and site of mutation was confirmed by X-ray crystallography for the most selective artificial metalloenzymes [η^5-(Biot-**2**)$RhCl_2$] **5** ⊂ K121H and [η^5-(Biot-**2**)$RhCl_2$] **5** ⊂ S112H. Current efforts are aimed at computing the transition state to identify and engineer additional second coordination sphere interactions to improve the catalytic performance of these dually-anchored artificial metalloenzymes.

Supporting Information. Modelling, biotinylated complex synthesis and characterization, catalytic runs and X-ray data. This material is available free of charge via the Internet at http://pubs.acs.org.

ACKNOWLEDGMENT

Generous support from the Canton of Basel, SNF (grant 200020_126366) as well as the Marie Curie training networks (BioChemLig FP7-ITN-238434 to TH and Biotrains FP7-ITN-238531 to EN) is gratefully acknowledged. TRW thanks Umicore for a precious metal loan as well as Prof. C. R. Cantor for the streptavidin gene.

REFERENCES

(1) Ward, T. R. *Acc. Chem. Res.* **2011**, *44*, 47.
(2) Rosati, F.; Roelfes, G. *ChemCatChem* **2010**, *2*, 916.
(3) Deuss, P. J.; den Heeten, R.; Laan, W.; Kamer, P. C. *Chem. Eur. J.* **2011**, *17*, 4680.
(4) Lu, Y.; Yeung, N.; Sieracki, N.; Marshall, N. M. *Nature* **2009**, *460*, 855.
(5) Abe, S.; Ueno, T.; Reddy, P. A. N.; Okazaki, S.; Hikage, T.; Suzuki, A.; Yamane, T.; Nakajima, H.; Watanabe, Y. *Inorg. Chem.* **2007**, *46*, 5137.
(6) Reetz, M. T. *Top. Organomet. Chem.* **2009**, *25*, 63.
(7) Wilson, M. E.; Whitesides, G. M. *J. Am. Chem. Soc.* **1978**, *100*, 306.
(8) Lin, C.-C.; Lin, C.-W.; Chan, A. S. C. *Tetrahedron Asymmetry* **1999**, *10*, 1887.
(9) Collot, J.; Gradinaru, J.; Humbert, N.; Skander, M.; Zocchi, A.; Ward, T. R. *J. Am. Chem. Soc.* **2003**, *125*, 9030.
(10) Reetz, M. T.; Peyeralans, J. J.-P.; Maichele, A.; Fu, Y.; Maywald, M. *Chem. Commun.* **2006**, 4318.
(11) Hyster, T. K.; Knörr, L.; Ward, T. R.; Rovis, T. *Science* **2012**, *338*, 500.
(12) Klein, G.; Humbert, N.; Gradinaru, J.; Ivanova, A.; Gilardoni, F.; Rusbandi, U. E.; Ward, T. R. *Angew. Chem. Int. Ed.* **2005**, *44*, 7764.
(13) Dürrenberger, M.; Heinisch, T.; Wilson, Y. M.; Rossel, T.; Nogueira, E.; Knörr, L.; Mutschler, A.; Kersten, K.; Zimbron, M. J.; Pierron, J.; Schirmer, T.; Ward, T. R. *Angew. Chem. Int. Ed.* **2011**, *50*, 3026.
(14) (a) Carey, J. R.; Ma, S. K.; Pfister, T. D.; Garner, D. K.; Kim, H. K.; Abramite, J. A.; Wang, Z.; Guo, Z.; Lu, Y. *J. Am. Chem. Soc.* **2004**, *126*, 10812. (b) Garner, D. K.; Liang, L.; Barrios, D. A.; Zhang, J.-L.; Lu, Y. *ACS Catal.* **2011**, *1*, 1083.
(15) Ohashi, M.; Koshiyama, T.; Ueno, T.; Yanase, M.; Fujii, H.; Watanabe, Y. *Angew. Chem. Int. Ed.* **2003**, *42*, 1005.
(16) Creus, M.; Pordea, A.; Rossel, T.; Sardo, A.; Letondor, C.; Ivanova, A.; LeTrong, I.; Stenkamp, R. E.; Ward, T. R. *Angew. Chem. Int. Ed.* **2008**, *47*, 1400.
(17) Zimbron, J. M.; Sardo, A.; Heinisch, T.; Wohlschlager, T.; Gradinaru, J.; Massa, C.; Schirmer, T.; Creus, M.; Ward, T. R. *Chem. Eur. J.* **2010**, *16*, 12883.
(18) Koehler, V.; Mao, J.; Heinisch, T.; Pordea, A.; Sardo, A.; Wilson, Y. M.; Knoerr, L.; Creus, M.; Prost, J.-C.; Schirmer, T.; Ward, T. R. *Angew. Chem., Int. Ed.* **2011**, *50*, 10863.
(19) Phillips, J. C.; Braun, R.; Wang, W.; Gumbart, J.; Tajkhorshid, E.; Villa, E.; Chipot, C.; Skeel, R. D.; Kale, L.; Schulten, K. *J. Comput. Chem.* **2005**, *26*, 1781.
(20) MacKerell Jr., A. D.; Brooks III, C. L.; Nilsson, L.; Roux, B.; Won, Y.; Karplus, M. *CHARMM: The Energy Function and Its Parameterization with an Overview of the Program*; John Wiley & Sons: Chichester, 1998; Vol. 1.
(21) Schmid, M.; Nogueira, E. S.; Monnard, F. W.; Ward, T. R.; Meuwly, M. *Chem. Sci.* **2012**, *3*, 690.
(22) Izrailev, S.; Stepaniants, S.; Balsera, M.; Oono, Y.; Schulten, K. *Biophys. J.* **1997**, *72*, 1568.
(23) Van Leusen, D.; Beetstra, D. J.; Hessen, B.; Teuben, J. H. *Organometallics* **2000**, *19*, 4084.
(24) Reiner, T.; Jantke, D.; Raba, A.; Marziale, A. N.; Eppinger, J. *J. Organomet. Chem.* **2009**, *694*, 1934.
(25) Amouri, H. E.; Gruselle, M.; Jaouén, G. *Synth. React. Inorg. Met.-Org. Chem.* **2010**, *24*, 395.
(26) Kaufman, T. *Tetrahedron Asymmetry* **2004**, *15*, 1203.
(27) Ogo, S.; Makihara, N.; Watanabe, Y. *Organometallics* **1999**, *18*, 5470.
(28) Canivet, J.; Süss-Fink, G.; Štěpnička, P. *Eur. J. Inorg. Chem.* **2007**, *2007*, 4736.
(29) Himeda, Y.; Onozawa-Komatsuzaki, N.; Sugihara, H.; Arakawa, H.; Kasuga, K. *J. Mol. Catal. A Chem.* **2003**, *195*, 95.

Graphical Abstract